Role of evaporation time on the structural and optical properties of ZnAlO composite films deposited by thermal evaporator

I. A. KHAN[a], M. NOOR[a], A. REHMAN[a], N. KANWAL[a], A. FARID[a], SADIA Z. BAJWA[b], WAHEED S. KHAN[b], M. A. K. SHAHID[c], M. SHAFIQ[d]

[a]*Department of Physics, Government College University Faisalabad, 38000, Faisalabad*
[b]*National Institute of Genetic Engineering and Biotechnology, 38000, Faisalabad*
[c]*Department of Physics, G P College of Science, Sammanabad, 38000, Faisalabad*
[d]*Department of Physics, QAU, Islamabad*

The polycrystalline zinc aluminum oxide (P-ZnAlO) composite films are deposited on Si for different (2 hrs, 3 hrs and 4 hrs) evaporation time (ET) by thermal evaporator. The XRD patterns confirm the development of different diffraction peaks related to ZnO (101, ZnO (002), ZnO (100) and Al_2O_3 (400) phases. The peak intensity of ZnO (100) plane is maximum when the film is deposited for 4 hrs ET. The crystallite size of Al_2O_3 (400) and ZnO (002) plane is found to be 25.43 nm and 11.58 nm whereas it is 14.72 nm for Al_2O_3 (400) plane and 33.65 nm for ZnO (100) plane for 3 and 4 hrs ET respectively. The decrease in crystallite size of Al_2O_3 (400) plane is associated with the orientation transformation of ZnO phase and re-arrangement of crystallites of Al_2O_3 (400) phase with increasing ET. The orientation transformation of ZnO phase is associated with the increase of ET. The dislocation density observed in different planes decreases with the increase of crystallite size. The SEM microstructure shows that the formation and growth of nano-particles having various shapes, sizes and distribution are associated with the increase of ET. The EDS spectrum confirms the presence of Zn, Al and O in the deposited P-ZnAlO composite films. The optical energy band gap of P-ZnAlO film varies from 3.39 eV to 3.9 eV with the increase of ET.

(Received May 05, 2015; accepted April 05, 2016)

Keywords: Polycrystalline; composite films, XRD; roughness; microstructure; nano-particles.

1. Introduction

Zinc oxide (ZnO) is a semiconductor material with wide energy band gap "*Eg*" (3.37 eV) and exciton binding energy (60 m eV) at room temperature [1-3]. The *Eg* of ZnO films can be tuned by alloying with other elements like Al and Mg resulted in the formation of ZnAlO and ZnMgO films respectively [4-7]. Moreover, pure ZnO is an n-type semiconductor material and its electrical and optical properties are not stable at high temperature [8, 9]. Due to this reason, for industrial and commercial usage, doped ZnO material in the form of thin film is characteristically preferred. Al is one of the best dopants, commonly used in growth process results in the formation of Al-doped ZnO films showing high quality and low-resistivity [10-15]. Al-doped ZnO is a key functional oxide that shows strong ultraviolet emission and high transparency to visible light and high conductivity. Al-doped ZnO is a transparent conducting oxide and it is being used as ideal candidate instead of tin-doped indium oxide commercially owing to its outstanding properties and its non-toxicity [16-19]. Al-doped ZnO films are being deposited by various deposition routes like thermal

evaporation, magnetron sputtering, chemical vapor deposition and pulsed laser deposition [20, 11, 12, 21-24].

In this study, the P-ZnAlO composite films are deposited by simple and cost-effective deposition technique so called thermal evaporator. The P-ZnAlO composite films are deposited for various evaporation (ET) times. The deposited P-ZnAlO films are characterized by x-ray diffraction (XRD), scanning electron microscope (SEM), energy dispersive x-ray spectroscopy (EDS), atomic force microscopy (AFM) and UV spectroscopy in order to explore the structural, morphological and optical properties of P-ZnAlO composite films.

2. Experimental setup

The P-ZnAlO composite films are deposited on Si substrates by thermal evaporator. The chamber is evacuated by rotary vane pump up to the pressure of 10^{-2} mbar. The chamber, made up of stainless steel, is filled with oxygen (1 mbar) pressure. Fig. 1 shows the schematic diagram of thermal evaporator. A digital temperature meter is employed to display the temperature of the

thermal evaporator plate (TEP). The deposition parameters like source to substrate distance (1 cm) and oxygen gas pressure (1 mbar) are fixed throughout the experiment. The P-ZnAlO composite films are deposited for different ET for the above mentioned fixed parameters. The basic mechanism behind the deposition of P-ZnAlO composite films is divided into two steps: (i) Zn powder (purity 99.9 %) placed on the TEP gets heat results in its evaporation and the ZnO films are deposited for different ET and (ii) Al powder (purity 99.9 %) placed on the TEP gets heat results in its evaporation and the AlO films are deposited on the ZnO films previously deposited in first step. The temperature of the TEP during step one is $420^{o}C$ while it is $660^{o}C$ during the second step. The flux of evaporated species of source materials may or may not react with the ionized oxygen species depending on their energies while travelling towards the substrate surface. We infer that the evaporated Zn and Al species may be of different energies which play an important role in the growth behavior of ZnO and AlO phases. The evaporated Zn and Al species react with ionized oxygen species to form their respective oxides which condensed on to the substrate surface in the form of thin film.
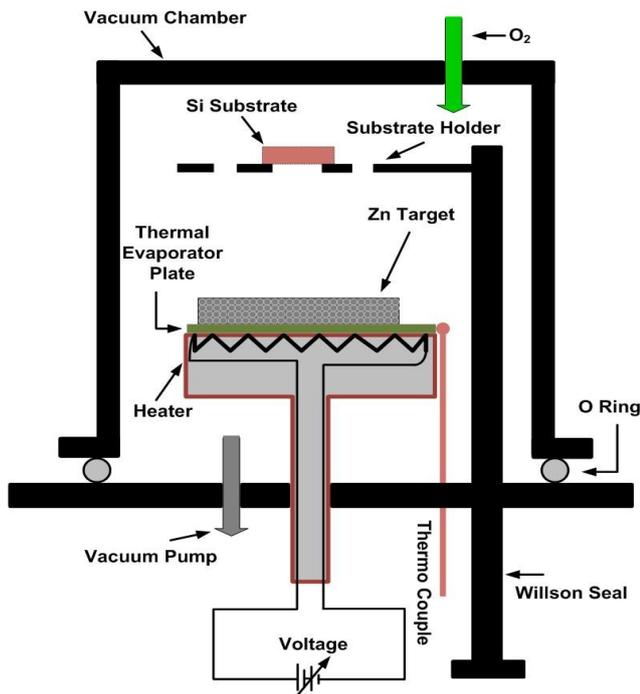

Fig. 1. The schematic diagram of thermal evaporator.

3. Structural analysis

The XRD pattern is used to investigate the crystal structure of P-ZnAlO composite films deposited for different ET. The crystallite size (C.S) of ZnO plane is estimated by using the formula [25, 26].

$$C.S = \frac{k\lambda}{\beta Cos\theta}$$

where k = 0.9 is a numerical constant, λ = 1.54 Å is the wavelength of x-rays and β is the full width at half maximum of the corresponding diffraction plane.

The strain (ε) developed in ZnO plane is estimated by using the relation [27].

$$\varepsilon = \frac{\beta Cos\theta}{4}$$

The dislocation density (δ) defined as the length of dislocation lines per unit volume of the crystal is estimated by employing the relation [27].

$$\delta = \frac{1}{(C.S)^2}$$

The lattice parameters of ZnO are estimated by using the relation [28]

$$n\lambda = 2dsin\theta$$

where n = 1, λ is the wavelength of x-rays and d is the spacing between two successive planes. Moreover, the d-spacing, lattice constant and *h k l* are connected through the relation [28].

$$\frac{1}{d_{(hkl)}^2} = \frac{4}{3}\left(\frac{h^2 + hk + k^2}{a^2}\right) + \frac{l^2}{c^2}$$

The bond length of ZnO is estimated by using the relation [26].

$$L = \sqrt{(\frac{a^2}{3} + (\frac{1}{2} - u)^2 c^2)} \quad \& \quad u = \frac{a^2}{3c^2} + 0.25$$

4. Results and discussions

4.1 Compositional analysis

The EDS spectrum is used for the quantitative analysis of P-ZnAlO composite films deposited for different ET. Table 1 shows the variation of elemental concentrations (Zn, Al and O) in the deposited P-ZnAlO composite films. It is found that the concentration of these elements is increased with the increase of ET. We assume that for 2 hrs ET, the Al content (0.22 at %) is not sufficient for the crystalline growth of the deposited film and even hinders the crystalline growth of ZnO phase results in the deposition of amorphous film.

Table 1. The concentration of different elements as a function of ET.

TT	Elemental Concentrations		
	Zn (at %)	Al (at %)	O (at %)
2 h	0.42	0.22	3.13
3 h	0.71	0.41	3.21
4 h	1.63	0.56	3.52

4.2 XRD analysis

Fig. 2 exhibits the XRD patterns of P-ZnAlO composite films deposited for different ET. For 2 hrs ET, no diffraction peak related to ZnO or Al_2O_3 phase is observed confirming the deposition of amorphous film. It shows that 2 hrs ET is not sufficient to crystalline any phase (ZnO or Al_2O_3). For 3 hrs ET, the XRD pattern exhibits the development of different diffraction peaks related to Al_2O_3 (400), ZnO (101) and ZnO (002) phase which confirms the deposition of P-ZnAlO composite films; however their peak intensities are weak. For 4 hrs ET, the peak intensity of Al_2O_3 (400) plane slightly increases while the ZnO (101) and (002) planes are disappeared along with the development of ZnO (100) plane. A strong diffraction peak of ZnO (100) plane is observed for 4 hrs ET. The orientation transformation in ZnO phase [from ZnO (101) or ZnO (002) to ZnO (100)] is also observed. It is interesting to note that both Al_2O_3 and ZnO phases are stable while the orientation transformation is observed only in ZnO phase for 4 hrs ET. Results show that if we provide constant temperature for longer time, the ZnO (101), (002) plane could not grow more; the re-crystallization occurs results in the orientation transformation to ZnO (100) plane. Therefore, the constant temperature for longer time plays an important role in the orientation transformation of ZnO phase. From the EDS and XRD analysis it is concluded that the relatively smaller Al (0.22 at. %) content hinders the growth of different diffraction plane of any phase results in the formation of amorphous film while for relatively larger Al (0.41 and 0.56 at. %) contents, the diffraction plane related to both Al_2O_3 and ZnO phases are observed results in the formation of crystalline film. Hence, the change in Al content plays a vital role to change the nature (amorphous or crystalline) and surface properties of the deposited P-ZnAlO composite film.
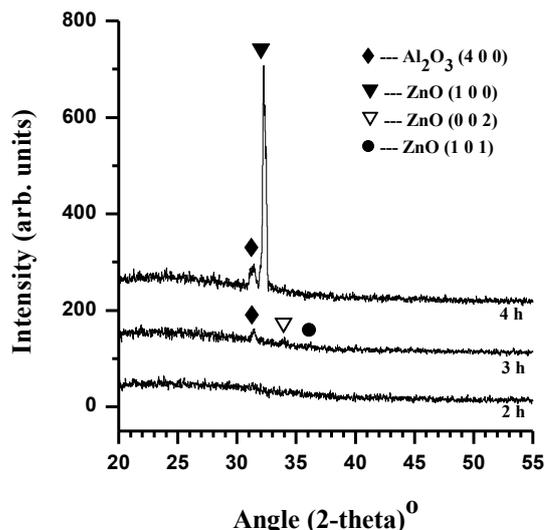

Fig. 2. The XRD patterns of P-ZnAlO composite films deposited for different ET.

Table 2 provides the information about the structural parameters like phase identification, *h k l* and 2θ values, FWHM, crystallite size, dislocation density, d-spacing, peak intensities and strain developed in different diffraction planes. For 3 hrs ET, the crystallite size of Al_2O_3 (400) and ZnO (002) is found to be 98.9 nm and 159.4 nm respectively. For 4 hrs ET, the crystallite size of Al_2O_3 (400) and ZnO (100) is found to be 58.63 nm and 79.35 nm respectively. It means that crystallite growth of ZnO (002) and ZnO (100) is more than Al_2O_3 (400) phase comparatively. The decrease in crystallite size of Al_2O_3 (400) shows its re-crystallization with increasing ET which is due to the better growth of ZnO phase because its peak intensity is increased.

For 3 hrs ET, the dislocation densities observed in Al_2O_3 (400) and ZnO (002) planes are found to be 1.02×10^{-4} nm^{-2} and 0.39×10^{-4} nm^{-2} respectively. For 4 hrs ET, the dislocation densities observed in Al_2O_3 (400) and ZnO (100) planes are found to be 2.91×10^{-4} nm^{-2} and 1.59×10^{-4} nm^{-2} respectively. The increase in dislocation densities is due to the orientation transformation of ZnO phase. The rearrangement of nano-particles during the orientation transformation is responsible to create vacancies and defects which cause to increase the dislocation density. The lattice parameters of ZnO film are found to be a = 3.198 nm and c = 5.258 nm which are agreed well with the literature values [a = 3.249 nm and c = 5.206 nm] [29, 30]. The deviation in the calculated and reported values of lattice parameter results in the elongation and contraction of crystal structure of ZnO which again confirms the development of defects and micro-strains.

Table 2. The structural parameters of P-ZnAlO composite films deposited for different ET.

TT	Phase	hkl	$2\theta_{st}$	$2\theta_{obs}$	FWHM	C.S (nm)	$\delta \times 10^{-3}$ (nm)$^{-2}$	I	d (nm)	Strain
3h	Al_2O_3	400	31.21	31.44	0.33	25.43	1.55	22.1	0.285	0.08
	ZnO	002	34.42	34.05	0.73	11.58	7.45	16.7	0.262	0.18
4h	Al_2O_3	400	31.21	31.44	0.57	14.72	4.62	46.1	0.285	0.14
	ZnO	100	31.77	32.27	0.25	33.65	0.90	460.7	0.277	0.06

The bond length of Zn-O is found to be 1.96 nm which is slightly higher than the reported value [31]. The increase in bond length is due to the incorporation of oxygen into Zn lattice intestinally. This increase in bond length is associated with the diffusion rate of oxygen ions into the Zn lattice. The incorporation of Al in Zn and ZnO lattice is the other reason to increase the bond length. Actually AlO which has higher young modulus attracts the oxides basically linked with Zn towards itself results in the elongation of Zn-O bond length.

The distance between cation-cation for hexagonal structure of ZnO is calculated by using the formula [32-34].

$$d_c = c \times \sqrt{\frac{3}{8}}$$

where c is the lattice parameter of hexagonal ZnO .

The calculated distance between cation-cation for Zn and O species is found to be 3.21 nm which is higher than the literature values [34] results in the elongation of Zn-O bond length and creation of defects and micro-strains. Table 3 shows the nature of P-ZnAlO composite films deposited for different ET. It is found that the increasing ET changes the nature (amorphous to crystalline) of the P-ZnAlO composite films.

Table 3. The nature of the P-ZnAlO composite films with increasing ET.

Evaporation times	Phases	Orientations	Nature of film
2 h	--------	--------	Amorphous
3 h	Al_2O_3 ZnO	(400) (002)	Crystalline
4 h	Al_2O_3 ZnO	(400) (100)	Crystalline

4.3 SEM analysis

The surface morphology of P-ZnAlO composite films deposited for different ET by thermal evaporator is investigated by SEM which provides the micro-structural information like size and shape of nano-particles, their distribution and the films compactness.
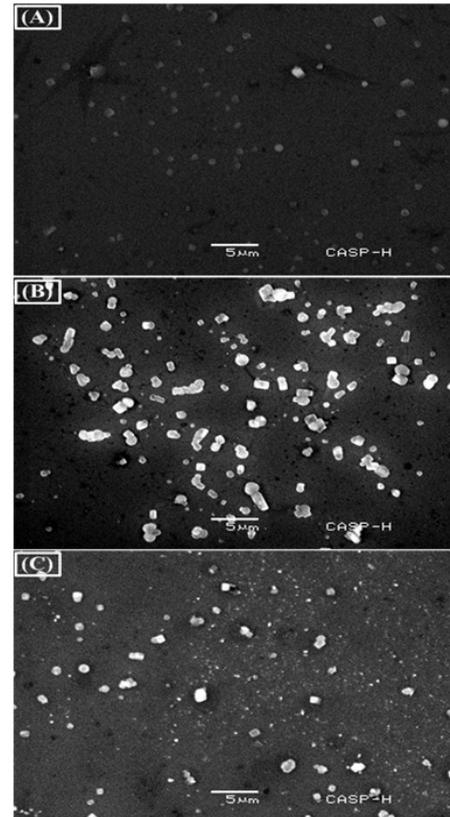

Fig. 3. The SEM microstructure of P-ZnAlO composite film deposited for (a) 2 hrs, (b) 3 hrs and (c) 4 hrs ET.

Fig. 3-A shows the SEM microstructure of P-ZnAlO composite film deposited for 2 hrs ET. The SEM images show the formation of square shape and rounded nano-particles distributed uniformly. The dimensions of rounded nano-particles are ranged from 385 nm to 1155 nm whereas the length of square shape nano-particles is ranged from 770 nm to 1151 nm. A compact film in the background of these nano-particles is also observed. Figure 3-B exhibits the SEM microstructure of P-ZnAlO composite film deposited for 3 hrs ET. The SEM microstructure again shows the formation of square shape, rounded and elongated nano-particles distributed uniformly. The dimensions of rounded nano-particles are ranged from 381 nm to 772 nm whereas the length of square type nano-particles is ranged from 761 nm to 1135 nm. The width and length of elongated nano-particles is ranged from 792 nm to 1541 nm and 1925 nm to 3850 nm respectively. The formation of irregular nano-pores of different diameters in the background of nano-particles is

observed. The clusters of nano-particles distributed uniformly are also observed. The amalgamation of nano-particles of diverse shapes and sizes make the surface rough. Figure 3-C demonstrates the SEM microstructure of P-ZnAlO composite film deposited for 4 hrs ET. The SEM microstructure again shows the formation of square shape and rounded nano-particles distributed uniformly. The dimensions of rounded nano-particles are ranged from 735 nm to 1524 nm whereas the length of square type nano-particles is found to be ~ 765 nm. Relatively a compact microstructure of P-ZnAlO composite film shows the formation of rounded nano-particles. In some regions, clusters of nano-particles are also observed. The formation of nano-particles of different dimensions on the top of the compact P-ZnAlO composite film makes the surface rough. It is concluded that the surface morphology like size, shape and distribution of nano-particles are associated with the increase of ET. The surface morphology of P-ZnAlO composite films depends on the provided time of evaporation for constant temperature.

4.4 AFM analysis

The nanostructures of P-ZnAlO composite films are also characterized by using SHIMADZU WET-SPM 9600 (Kyoto, Japan). Each AFM image at least from three different areas using the same tip is taken. For scans, silicon nitride atomic force microscopy (model OMCL-TR800PSA-1) having micro-cantilever with 100 μm thickness with force constants of 0.57 N/m is employed. The resonance frequency is adjusted to be 73 kHz. All the scans are carried in ambient temperature in contact mode. The SPM Manager Software attached with the AFM system is used for the data analysis.

The AFM scans are also employed to understand the surface roughness of P-ZnAlO composite films deposited for different ET. The AFM image (figure 4-A) of P-ZnAlO composite film deposited for 2 hrs ET shows the formation of cones of different heights and widths. In the background of these cones, the strips of different widths and heights are also observed. However, the cones could not cover the whole scanned surface along with the formation of deep-niche between the strips which makes the surface rough. For 3 and 4 hrs ET, again the cones of different heights and widths are observed; however, the covered area by the cones is more for 3 hrs ET comparatively. It is concluded that the formation of cones, their widths and growth and film compactness are associated with increase of ET.

Fig. 5 exhibits the variation in surface roughness of P-ZnAlO composite films deposited for different ET. The surface roughness of P-ZnAlO composite film is increased from 32 nm to 72 nm up to 3 hrs ET, after that it starts to decrease. The minimum surface roughness of P-ZnAlO composite film is observed for 4 hrs ET. The trend in the variation of surface roughness is inverted cup like shape. The maximum surface roughness of P-ZnAlO composite film is due to the development of different phases and the formation of nano-particles (XRD results). We may predict that the minimum surface roughness of P-ZnAlO composite film deposited for 4 hrs ET is due to the better

growth of ZnO phase. However, randomly distributed nano-particles which do not shows crystalline patterns but closely packed is also responsible to reduce the surface roughness of P-ZnAlO composite film deposited for 2 hrs ET.
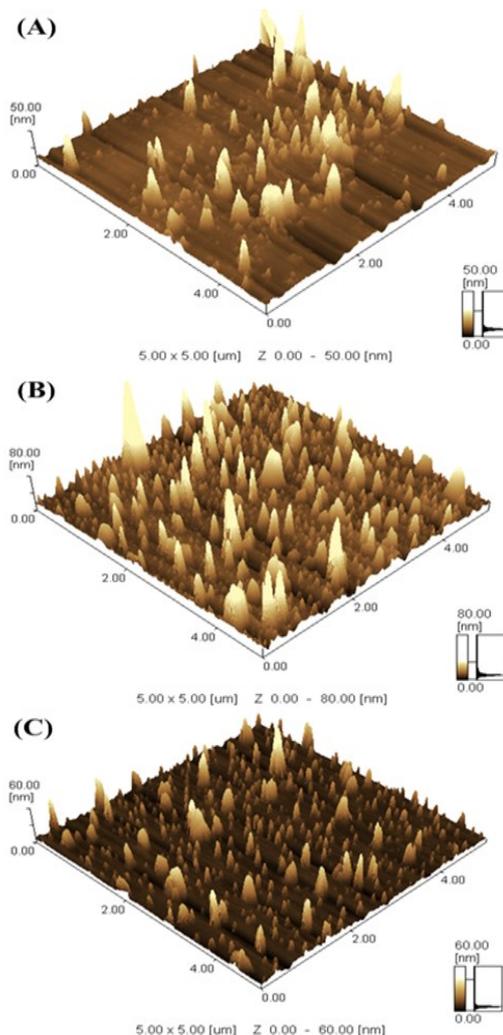

Fig. 4. The AFM images of the P-ZnAlO composite films deposited for (a) 2 hrs, (b) 3 hrs and 4 hrs ET.

Moreover, for 3 hrs ET, the weak and broadened peak intensities reduce the crystallite size and increase the crystallite boundary area which in turn increases the surface roughness and mechanical properties of the P-ZnAlO composite film. For 4 hrs ET, the increase in peak intensity and the decrease in FWHM minimize the crystallite boundary area results in the reduction of film surface roughness.

The ZnO is a semiconductor material and its surface roughness may play an important role to change the performance of inverted solar cell (ISCs) materials. Ma et al. have studied the influence of surface roughness of ZnO interlayer used as electron transporting interlayer in organic inverted solar cells (ISCs) and their performance. They found that the fill factor, short-circuit photocurrent density and open-circuit voltage of ISCs were increased from 0.58 to 0.65, 5.60 to 7.02 mA/cm^2 and 0.83 to 0.85 V

when the surface roughness of ZnO layer was decreased from 48 nm to 1.9 nm respectively and the power conversion efficiency of ISCs was increases from 2.7% to 3.9% when the surface roughness of ZnO layer was decreased from 48 nm to 1.9 nm [35].

In our case, the surface roughness of ZnAlO layers is ranged from 30 nm to 72 nm when it is deposited for 2 hrs to 4 hrs ET whereas it is 72 nm when deposited for 3 hrs ET. The surface roughness of ZnAlO layers deposited for 2 hrs and 4 hrs ET is approximately equal to 30 ± 2 nm which is less than 48 nm and greater than 1.9 nm of the surface roughness values of ZnO layer [35]. We propose that the value of fill factor, short-circuit photocurrent density and open-circuit voltage of ZnAlO layer deposited for 2 hrs and 4 hrs ET should be greater than 0.58, 5.60 mA/cm^2, 0.83 V and 2.7 % values but smaller when the ZnAlO layer is deposited for 3 hrs ET because these values were reported for ZnO layer having surface roughness 48 nm. Therefore the ZnAlO films deposited by thermal evaporator should be used as ISC. However, the co-existence of Al$_2$O$_3$ and ZnO phases and their growth behavior with increasing ET are responsible to increase the surface roughness. Thus the growth behavior and co-existence of Al$_2$O$_3$ and ZnO phases are responsible to change the film surface roughness which definitely affect on the performance of ZnAlO layer when used in solar cell applications.

4.5 UV analysis

The optical characterization of P-ZnAlO composite films provides the information about the optical energy (E$_g$) band gap. The absorption spectrum is used to calculate the E$_g$ value of P-ZnAlO composite films. The absorption coefficient (α) can be determined by using the relation [36, 37].

$$\alpha = \frac{2.303\,A}{t}$$

where A is the absorbance and t is the film thickness. The estimated film thickness is ranged from 1100 to 1300 nm with increasing ET.

The relation between α and incident photon energy ($h\upsilon$) is given by the relation [38, 39].

$$\alpha h\upsilon = A\,(h\upsilon - E)^n$$

where *B* is a constant which does not depend on the photon energy, *E* is the band gap energy, $h\upsilon$ is the photon energy and the exponent *n* depends on the material. For direct band gap semiconductor material, the exponent n = 1/2 or 2/3 and n = 1/2 is more suitable for ZnO because it provides the appropriate linear plot between photon energy and $\alpha h\upsilon$ [40]. The extrapolating of the straight line portion (which cut the x-axis) of the plot between $(\alpha h\upsilon)^2$ and (hυ) gives the E$_g$ value of P-ZnAlO composite films.

Fig. 6 reveals the absorbance spectra of P-ZnAlO composite films deposited for different ET. The maximum absorption occurs at the wavelength of 295 nm for 2 hrs which reduces with the increase of ET. A strong

absorption occurs in the wavelength ranged from 295 nm to 355 nm whereas weak absorption is observed for the wavelength ranged from 400 nm to 700 nm.

Fig. 7 shows the E$_g$ values of P-ZnAlO composite films deposited for different ET. The E$_g$ values of P-ZnAlO composite films are increased from 3.39 eV, 3.5 eV and 3.91 eV with the increase of ET. The E$_g$ value of P-ZnAlO composite film deposited for 2 hrs ET is close to the reported values [41]. During the switching of the nature of P-ZnAlO composite film (from amorphous to crystalline), the rearrangement of nano-particles takes place leaving vacancies results in the increase of E$_g$ values. The increase in E$_g$ value is also due to the orientation transformation [from ZnO (002) to ZnO (100)]. Thus, it is concluded that the switching of the film nature (from amorphous to crystalline) and the orientation transformation in ZnO phase are responsible to increase the E$_g$ value of P-ZnAlO composite films. The incorporation of Al in ZnO lattice and the creation of oxygen vacancies during the deposition process may be the other reasons. However, the variation in these parameters is associated with the increase of ET.
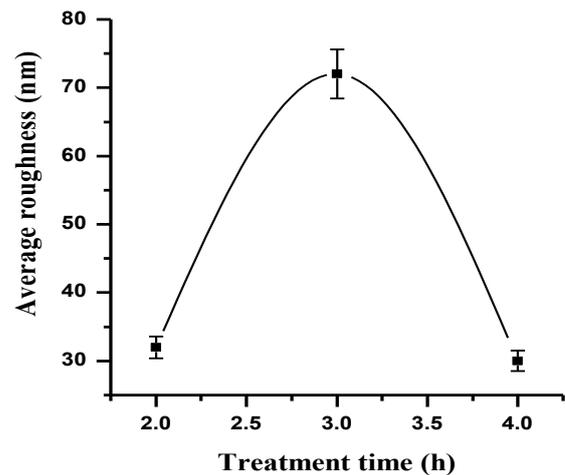

Fig. 5. The variation in surface roughness of P-ZnAlO films deposited for different ET.
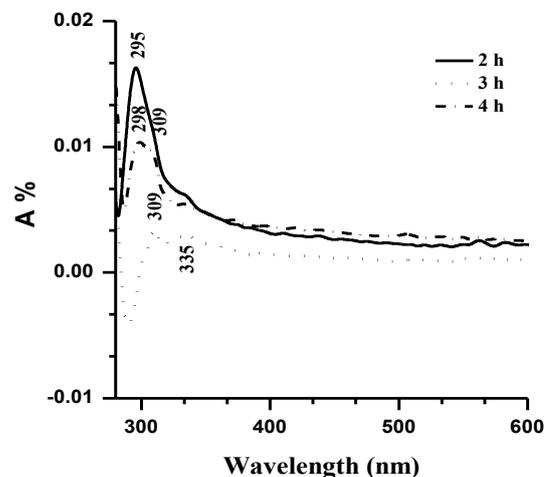

Fig. 6. The absorption spectra of P-ZnAlO composite films deposited for various ET.

In our case, the P-ZnAlO composite films are deposited for constant temperature but for different ET. We hypothesized that the increasing ET increases the rearrangement of involved species and nano-particles of newly formed phase's results in the variation of E_g values of P-ZnAlO composite films. Table 4 shows that the E_g values of P-ZnAlO composite film increases while its average crystallite size is decreased with the increase of ET.

We assumed that the increasing ET behaves like the increasing annealing temperature and the increasing annealing temperature enhances the E_g of P-ZnAlO composite films [42]. It is well known that the E_g value of ZnO films was increased by decreasing the diameter of nano-rods and the diameter of nano-rods was decreased with increasing annealing temperature [42]. In our case, the decrease in average crystallite size of P-ZnAlO composite films with increasing ET is responsible to enhance the E_g values. Moreover, the increasing ET, oxygen vacancies, the orientation transformation of ZnO phase and the combination of AlO and ZnO phases are responsible to increase the E_g values of P-ZnAlO composite films.
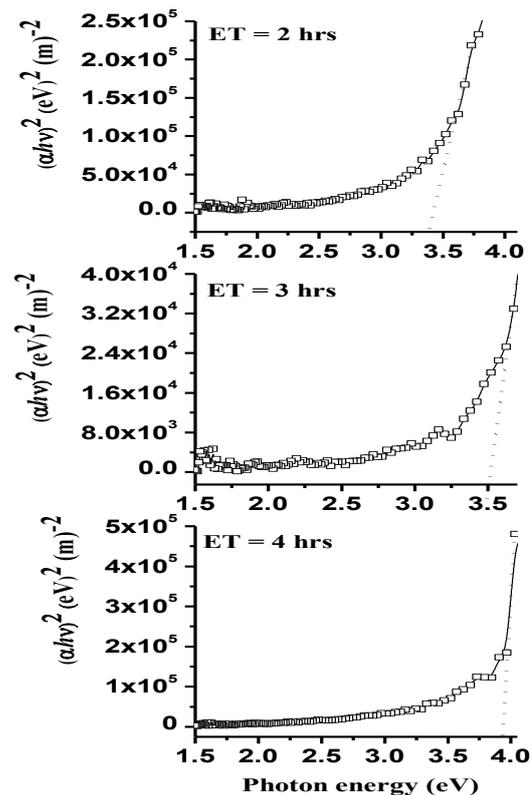

Fig. 7. The E_g of P-ZnAlO composite film deposited for 2, 3 and 4 hrs ET.

Table 4. The different parameters of P-ZnAlO composite films as a function of ET.

Evaporation times	Phase	h k l	C.S (nm)	A.C.S (nm)	E_g (eV)	ʎ (nm)
2 h	------	------	-------	-----	3.39	295
3 h	Al_2O_3	400	98.9	129.15	3.5	298
	ZnO	002	159.4			309
4h	Al_2O_3	400	58.63	68.99	3.9	309
	ZnO	100	79.35			355

5. Conclusions

The P-ZnAlO composite films are deposited on Si for different ET by thermal evaporator. The XRD patterns confirm the deposition of amorphous and P-ZnAlO composite films. The average crystallite size of Al_2O_3 (400) and ZnO (100) are found to be 58.63 nm and 79.35 nm respectively. For 4 hrs ET, the ZnO phase is more than Al_2O_3 phase in the deposited P-ZnAlO composite film. The dislocation densities observed in different diffraction planes are increased with the increase of ET. The orientation transformation of ZnO phase is responsible to increase the dislocation densities. The lattice parameters of ZnO film are found to be a = 3.198 Å and c = 5.258 Å. The bond length of ZnO and the cation-cation distance between Zn and O species are found to be 1.96 nm and 3.21 nm respectively. The peak intensity of various diffraction planes, the orientation transformation of ZnO phase and the average crystallite size are associated with the increase of ET. The SEM analysis shows the formation of square and rounded shape nano-particles; however their size, shape and distribution are attributed with the increase of ET. The AFM analysis confirms the formation of cones like microstructures and the estimated values of surface roughness are found to be ~ 32 nm, ~ 72 nm and ~ 30 nm for 2 hrs, 3 hrs and 4 hrs ET respectively. The EDS analysis confirms the presence of Zn, Al and O in the deposited P-ZnAlO composite films and their concentrations are associated with the increase of ET. The E_g values of the P-ZnAlO composite films deposited for 2 hrs, 3 hrs and 4 hrs ET are found to be 3.39 eV, 3.5 eV and 3.9 eV respectively. These P-ZnAlO composite films are being used as semiconductor material for solar cell applications due to larger energy band gap.

References

[1] Z.K. Tang, G.K.L. Wong, P. Yu, M. Kawasaki, A. Ohtomo, H. Koinuma, Y. Segawa, Appl. Phys. Lett. **72**, 3270 (1998).

[2] D.C. Look, D.C. Reynolds, J.R. Sizelove, R.L. Jones, C.W. Litton, G. Cantwell, W.C. Harsch, Solid State Commun. **105**, 399 (1998).

[3] D.M. Bagnall, Y.F. Chen, Z. Zhu, T. Yao, S. Koyama, M.Y. Shen, T. Goto, Appl. Phys. Lett. **70**, 2230 (1997).

[4] A. Ohtomo, *et al.* Appl. Phys. Lett. **72**, 2466 (1998).

[5] K. Koike, K. Hama, I. Nakashima, G. Takada, K. Ogata, S. Sasa, M. Inoue, M. Yano, J. Cryst. Growth **278**, 288 (2005).

[6] T. Makino, Y. Segawa, M. Kawasaki, A. Ohtomo, R. Shiroki, K. Tamura, T. Yasuda, H. Koinuma, Appl. Phys. Lett. **78**, 1237 (2001).

[7] Z.Z. Ye, D.W. Ma, J.H. He, J.Y. Huang, B.H. Zhao, X.D. Luo, Z.Y. Xu, J. Cryst. Growth **256**, 78 (2003).

[8] G. Xiong, J. Wilkinson, B. Mischuck, S. Tüzemen, K.B. Ucer, R.T. Williams, Appl. Phys. Lett. **80**, 1195 (2002).

[9] V. Gupta, A. Mansingh, J. Appl. Phys. **80**, 1063 (1996).

[10] B.J. Lokhande, P.S. Patil, M.D. Uplane, Physica B **302/303**, 59 (2001).

[11] D.J. Cohen, K.C. Ruthe, S. A. Barnett, J. Appl. Phys. **96**, 459 (2004).

[12] S.S. Lin, J.L. Huang, P. Šajgalik, Surf. Coat. Technol. **185**, 254 (2004).

[13] T. Makino, Y. Segawa, S. Yoshida, A.Tsukazaki, A. Ohtomo, M. Kawasaki, Appl. Phys. Lett. **85**, 759 (2004).

[14] T. Agne, Z. Guan, X.M. Li, H. Wolf, T. Wichert, H. Natter, R. Hempelmann, Appl. Phys. Lett. **83**, 1204 (2003).

[15] T. Minami, H. Sato, H. Nanto, S. Takata, Jpn. J. Appl. Phys. Part 2, **25**, L776 (1986).

[16] H. Kim, J.S. Horwitz, G.P. Kushto, Z.H. Kafafi, D.B. Chrisey, Appl. Phys. Lett. **79**, 284 (2001).

[17] D. Song, A.G. Aberle, J. Xia, Appl. Surf. Sci. **195**, 291 (2002).

[18] F. Zhuge, et al., Appl. Phys. Lett. **87**, 092103 (2005).

[19] J.G. Lu, L.P. Zhu, Z.Z. Ye, F. Zhuge, B.H. Zhao, L. Wang, J.Y. Huang, J. Yuan, J. Cryst. Growth **283**, 413 (2005).

[20] J. Ma, F. Ji, D.H. Zhang, H.L. Ma, S.Y. Li, Thin Solid Films **357**, 98 (1999).

[21] A. Martín, J.P. Espinós, A. Justo, J.P. Holgado, F. Yubero, A.R. González-Elipe, Surf. Coat. Technol. **151/152**, 289 (2002).

[22] J. Mass, P. Bhattacharya, R.S. Katiyar, Mater. Sci. Eng. B **103**, 9 (2003).

[23] H. Kim, et al., Appl. Phys. Lett. **76**, 259 (2000).

[24] M. Kumar, R.M. Mehra, A. Wakahara, M. Ishida, A. Yoshida, J. Appl. Phys. **93**, 3837 (2003).

[25] G.K. Williamson, R.E. Smallman, Philosophical Magazine **1**, 34 (1956).

[26] X.S. Wang, Z.C. Wu, J. F. Webb, Z.G. Liu, Appl. Phys. **77**, 561 (2003).

[27] Z.R. Khan, M. Zulfequar, M.S. Khan, Mater. Sci. Eng. B **174**, 145 (2010).

[28] B.D. Cullity, S. Rstock, Elements of X-ray Diffraction, Prentice Hall, New Jersey (2001).

[29] Z.W. Li, W. Gao, R.J. Reeves, Surf. Coat. Technol. **198**, 319 (2005).

[30] Q.P. Wang, X.J. Zhang, C.Q. Wang, S.H. Chen, X.H. Wu, H.L. Ma, Appl. Surf. Sci. **254**, 5100 (2008).

[31] D. I. Rusu, G.G. Rusu, D. Luca, Acta Physica Plonica A, 119 (2011) 850

[32] J. Tauc, R. Grigorovici, Y. Vancu, Phys. Status. Solidi. **15**, 627 (1966).

[33] J. Mass, P. Bhattacharya, R.S. Katiyar, Mater Sci. Eng. B **9**,103 (2003).

[34] D.I. Rusu, G.G. Rusu, D. Luca, ACTA Physica Polonica A **119**, 1 (2011).

[35] Zaifei Ma, Zheng Tang, Ergang Wang, Mats R. Andersson, Olle Ingana, Fengling Zhang, J. of physical chemistry C, 116, 2012, 24462-68

[36] K.B. Kumar, P. Raji, Recent Research in Science and Technology **3**, 48 (2011).

[37] M-F. Li, Modern Semiconductor Quantum Physics, World Scientific, Singapore (2001).

[38] N. Nithya, S.R. Radhakrishnan, Advance Appl. Sci. **3**, 4041 (2012).

[39] S.S. Shariffudin, M. Salina, S.H. Herman, Transactions on Electrical and Electronic Materials **13**, 102 (2012).

[40] S.W. Xue, X.T. Zu, W.L. Zhouc, H.X. Denga, X. Xiang, L. Zhang, H. Deng, J. of Alloys & Compounds **448**, 21 (2008).

[41] V. Senay, S. Pat, S. Korkmaz, T. Aydogmus, S. Elmas, S. Ozen, N. Ekem, M. Zafer, Appl. Surf. Sci, **314**, 2 (2013).

[42] H.A. Wahab, A.A. Salama, A.A. El-Saeid, O. Nur, M. Willander, I.K. Battisha, Results in Physics **3**, 46 (2013).

[*]Corresponding author: ijazahmad@gcuf.edu.pk